Electronic Supplementary Material (ESI) for RSC Advances.


**Supporting Information**

# Greatly enhanced hole collection of MoOx with top sub-10 nm thick silver films for gridless and flexible crystalline silicon heterojunction solar cells

Qiyun Lei,[a, †] Xinan Xu,[a, †] Na Lu,[a] Liu Yang*[a,b] and Sailing He*[a,b,c]

[a.] *Centre for Optical and Electromagnetic Research, National Engineering Research Center for Optical Instruments, Zhejiang University, Hangzhou 310058, China. E-mails: optyang@zju.edu.cn; sailing@zju.edu.cn*

[b.] *Ningbo Research Institute, Zhejiang University, Ningbo 315100, China.*

[c.] *JORCEP, School of Electrical Engineering, Royal Institute of Technology (KTH), S-100 44 Stockholm, Sweden.*

**Note S1. Demonstration of the importance of the drying process in an air-oven at 90 ℃ for 10 min after HF etching**

After thorough cleaning, an oxide layer was produced on the surfaces of the c-Si wafer and removed by the following HF etching. Subsequently, before being transferred to the vacuum chamber of the thermal evaporator, the wafer was dried in an oven at 90 ℃ for 10 min. Since air was in the oven, another oxide thin layer must regrow on the surfaces of the wafer. In order to verify the necessity of this drying process, we fabricated two c-Si heterojunction solar cells with and without the drying process. The HSCs of the two cells were $MoO_x$/8-nm Ag HSCs and the ESCs were $LiF_x$/Al ESCs. The measured J-V curves are shown in Fig. S1 and the characteristic parameters are listed in Table S1. With the drying process, the fabricated solar cell demonstrates enhancements in $J_{sc}$, $V_{oc}$ and PCE with a negligible reduction in FF. This clearly illustrates that the drying process is of great necessity to improve the interfacial qualities between c-Si and $LiF_x$ as well as between c-Si and $MoO_x$, and hence the power conversion performance of the device.

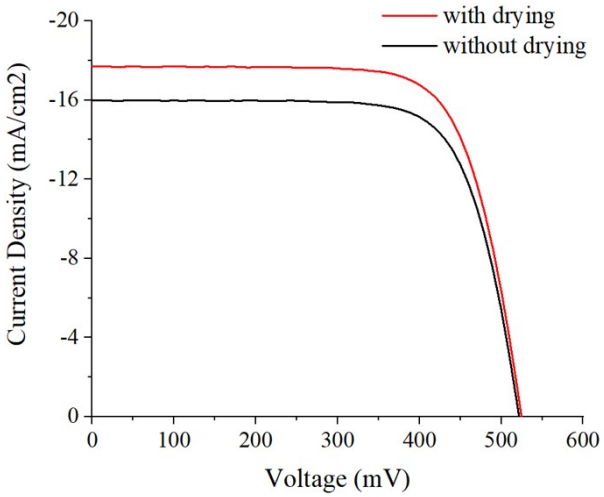


**Fig. S1** Measured J-V curves of the 200-μm thick c-Si heterojunction solar cells fabricated with and without the drying process.

**Table S1** The characteristic parameters of the 200-μm thick c-Si heterojunction solar cells fabricated with and without the drying process extracted from the measured J-V curves shown in Fig. S1.

| 200-μm thick c-Si solar cells | $J_{sc}$ (mA/cm$^2$) | $V_{oc}$ (mV) | FF (%) | PCE (%) | Shunt Resistance (Ω·cm$^2$) | Series Resistance (Ω·cm$^2$) |
|---|---|---|---|---|---|---|
| With drying | 17.69 | 524.4 | 72.99 | 6.77 | 1243.8 | 3.99 |
| Without drying | 16 | 522.1 | 73.2 | 6.11 | 1154.7 | 3.88 |

**Note S2. Transfer length method**

The contact property between the hole-selective contact (HSC) and the n-type Si was characterized with a transfer length method [S1]. As shown in Fig. S2, when a voltage (V) is applied to the Ag line pads, a current (I) can be measured, flowing from one pad to another. If Ohmic contacts are formed at the HSC/Si interfaces, the current will vary linearly with the voltage. The total resistance, $R_{tot}$, between the two pads can be derived easily from the slope of the linear I-V curve.

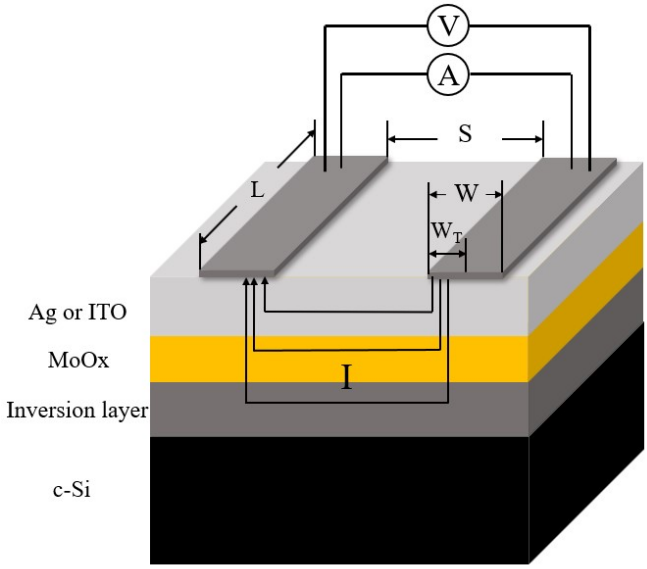


Fig. S2. Schematic diagram of the transfer length method for contact property characterization.

Actually, $R_{tot}$ originates mainly from the in-plane resistance, $R_{ip}$, between the pads and the contact resistance, $R_c$, under the pads. Assuming the same $R_c$ of the two pads, $R_{tot}$ is expressed below:

$$R_{tot} = \frac{V}{I} = R_{ip} + 2R_c \tag{1}$$

where, $R_{ip} = R_{sh\_HSC} \cdot S/L$, $R_{sh\_HSC}$ is the sheet resistance between the two pads, S and L are the pad spacing and length, respectively. Since the current can pass through the single layer or double layers of the HSC and also the inversion layer immediately under the HSC, $R_{sh\_HSC}$ is an overall sheet resistance of both the HSC and the inversion layer.

At the HSC/Si interface, if $R_c$ is small enough, only part of the pad is used for current flow. In this case, the effective width, $W_T$, is smaller than the physical width, W, of the pad (Fig. S2), and $R_c$ can be expressed below:

$$R_c = \frac{\rho_{c\_HSC}}{W_T L} = \frac{\sqrt{\rho_{c\_HSC} R_{sh\_HSC}}}{L} \tag{2}$$

On the other hand, if $W_T$ is larger than W, the whole pad is used for current flow, and $R_c$ is expressed below:

$$R_c = \frac{\rho_{c\_HSC}}{WL} \tag{3}$$

In Eqs. (2) and (3), $\rho_{c\_HSC}$ is the contact resistivity of the HSC/Si interface, which is also an overall

parameter representing all the factors along the current flow vertically from the Ag pad to the HSC under the pad and to the inversion layer immediately under the HSC.

By changing the pad spacing, S, we can measure a series of linear I-V curves and plot the extracted $R_{tot}$ as a function of S, as shown in Fig. 2a, 2b and 2c for the three HSCs. According to Eqs. (1)-(3), $R_{tot}$ varies linearly with S, and can be fitted with a straight line. From the slope and the intersection with the vertical axis of the $R_{tot}$-S fitting line, both $R_{sh\_HSC}$ and $\rho_{c\_HSC}$ can be easily derived, respectively.

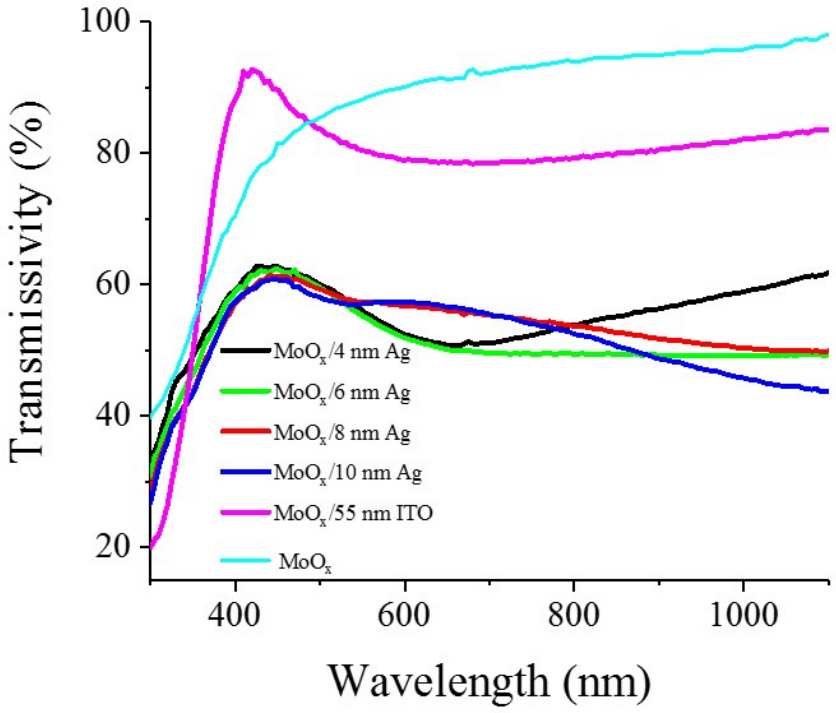


**Fig. S3**. Measured optical transmission spectra of Ag films with different thicknesses a ~ 55-nm thick ITO on quartz substrates coated with ~ 23-nm thick $MoO_x$ layers. All the spectra are normalized to that of the quartz substrate.

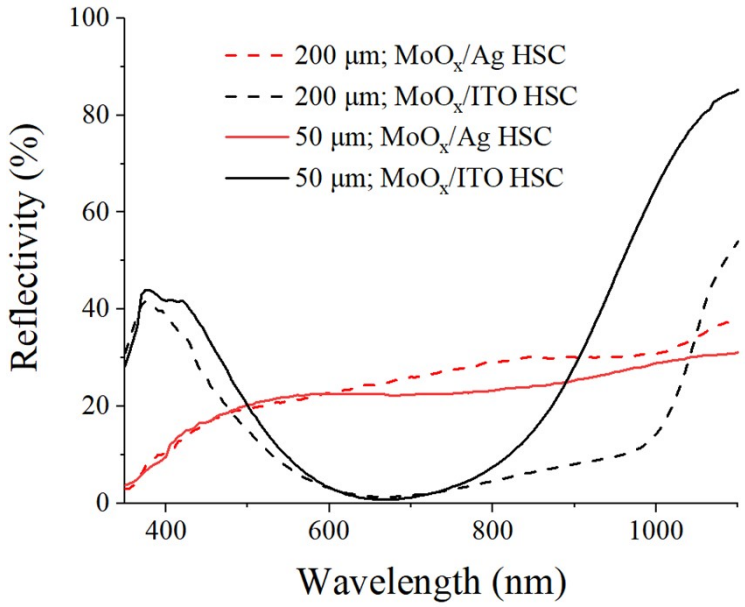


**Fig. S4**. Measured reflectivity spectra of the 50- and 200-μm thick c-Si heterojunction solar cells with $MoO_x$/8-nm Ag and $MoO_x$/55-nm ITO HSCs.

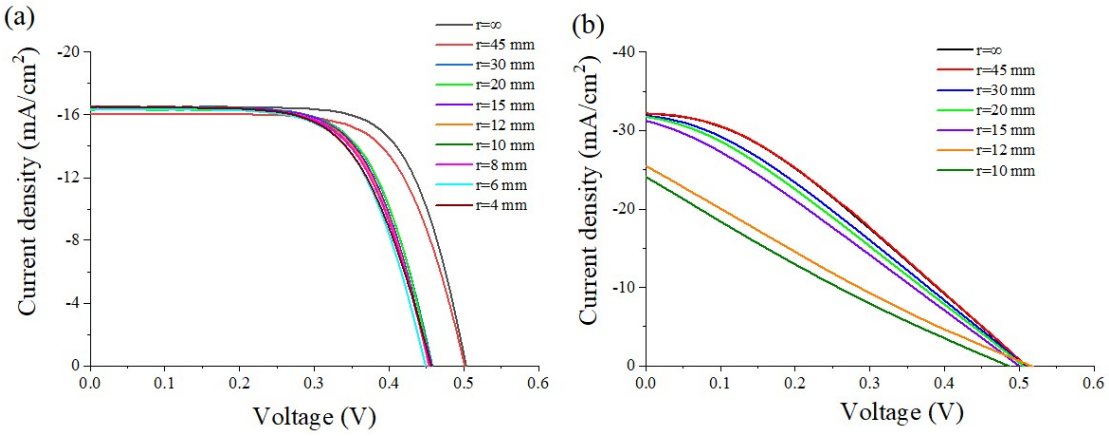


**Fig. S5**. Measured J-V curves of the 50-μm thick c-Si heterojunction solar cells with (a) the $MoO_x$/8-nm Ag HSC and (b) the $MoO_x$/55-nm ITO HSC, being bent at different curvature radii, r.

**Table S2** Comparison of the contact resistivities of the $MoO_x$/8-nm Ag, $MoO_x$/55-nm ITO, and pure $MoO_x$ HSCs to the n-type c-Si in our work, as well as the contact resistivities of previously-reported HSCs to either n-type or p-type c-Si.

| **HSCs** | **$\rho_{c\_HSC}$ ($\Omega$*cm$^2$)** | **References** |
|---|---|---|
| 8-nm Ag/$MoO_x$/n-Si | 0.053 | This work |
| 55-nm ITO/$MoO_x$/n-Si | 0.114 | This work |
| $MoO_x$/n-Si | 2.56 | This work |
| $MoO_x$/n-Si | 0.1 | S1 |
| Ag/$MoO_{3-x}$:V/n-Si | 2.1 | S2 |
| Ag/ITO/$MoO_x$/n-Si | 0.385 | S3 |
| Ag/$MoO_x$/a-Si:H(i)/n-Si | 0.224 | S4 |
| $MoO_x$/n-Si | 0.0785 | S5 |
| Ag/$MoO_x$/n-Si | 0.0559 | S6 |
| Ag/s-$MoO_x$[a]/n-Si | 5.6 | S7 |
| Ag/ALD[b] $MoO_x$/p-Si | 0.38 | S8 |
| $MoO_x$/p-Si | 0.32 | S9 |
| Al/Ni/$MoO_x$/p-Si | <0.01 | S10 |
| $MoO_x$/p-Si | 0.053 | S11 |
| ALD[b] $VO_x$/n-Si | 0.095 | S12 |
| ALD[b] $V_2O_5$/n-Si | 0.25 | S13 |
| Ag/$WO_x$/$V_2O_x$/p-Si | 0.061 | S14 |
| Ag/Cu:$CrO_x$/p-Si | 0.095 | S15 |

[a]Solution-processed $MoO_x$; [b]Atomic layer deposition.

**References**

[S1] J. Bullock, A. Cuevas, T. Allen and C. Battaglia, *Applied Physics Letters*, 2014, **105**, 232109.

[S2] C. Liu, L. Zhang, G. Yu, T. Wang, X. Wu, L. Xu, P. Lin, C. Cui, X. Yu and P. Wang, Materials Science in Semiconductor Processing, 2022, 146, 106687.

[S3] M. Nayak and V. K. Komarala, IEEE Transactions on Electron Devices, 2022, 69, 3251-3257.

[S4] W. Wang, J. He, D. Yan, W. Chen, S. Pheng Phang, C. Samundsett, S. Krishna Karuturi, Z. Li, Y. Wan and W. Shen, Solar Energy, 2022, 231, 203-208.

[S5] J. Chen, C. Liu, S. Xu, P. Wang, X. Ge, B. Han, Y. Zhang, M. Wang, X. Wu, L. Xu, P. Lin, X. Huang, X. Yu and C. Cui, Materials Science in Semiconductor Processing, 2021, 132, 105920.

[S6] M. Gülnahar, H. Nasser, A. Salimi and R. Turan, Journal of Materials Science: Materials in Electronics, 2021, 32, 1092-1104.

[S7] C. Lu, Rusli, A. B. Prakoso and Z. Li, Materials Chemistry and Physics, 2019, 236, 121779.

[S8] T. Pan, J. Li, Y. Lin, Z. Xue, Z. Di, M. Yin, J. Wang, L. Lu, L. Yang and D. Li, Journal of Materials Science: Materials in Electronics, 2021, 32, 3475-3486.

[S9] Y. Jiang, S. Cao, L. Lu, G. Du, Y. Lin, J. Wang, L. Yang, W. Zhu and D. Li, Nanoscale Research Letters, 2021, 16, 87.

[S10] G. Gregory, C. Luderer, H. Ali, T. S. Sakthivel, T. Jurca, M. Bivour, S. Seal and K. O. Davis, Advanced Materials Interfaces, 2020, 7, 2000895.

[S11] H. Nasser, F. Es, M. Zolfaghari Borra, E. Semiz, G. Kökbudak, E. Orhan and R. Turan, Progress in Photovoltaics: Research and Applications, 2021, 29, 281-293.

[S12] X. Yang, H. Xu, W. Liu, Q. Bi, L. Xu, J. Kang, M. N. Hedhili, B. Sun, X. Zhang and S. De Wolf, Advanced Electronic Materials, 2020, 6, 2000467.

[S13] G. Masmitjà, E. Ros, R. Almache-Hernández, B. Pusay, I. Martín, C. Voz, E. Saucedo, J. Puigdollers and P. Ortega, Solar Energy Materials and Solar Cells, 2022, 240, 111731.

[S14] Z. Liu, W. Lin, Z. Chen, D. Chen, Y. Chen, H. Shen and Z. Liang, Advanced Materials Interfaces, 2022, 9, 2102374.

[S15] Z. Xu, S. Peng, H. Lin, S. Tian, Z. Wang, J. He, L. Cai, J. Hou and P. Gao, Solar RRL, 2021, 5, 2100064.